Author for correspondence:
Clare Eayrs,
E-mail: clare.eayrs@nyu.edu

Mechanisms driving the asymmetric seasonal cycle of Antarctic Sea Ice in the CESM Large Ensemble

Clare Eayrs[1] , Daiane Faller[1] and David M. Holland[1,2]

[1]Center for Global Sea Level Change, New York University Abu Dhabi, United Arab Emirates and [2]Center for Atmosphere Ocean Science, Courant Institute of Mathematical Sciences, New York University, USA

Abstract

The yearly paired process of slow growth and rapid melt of some 15 million square kilometers of Antarctic sea ice takes place with a regular asymmetry; the process has been linked to the relationship of the position of the ice edge with the band of low pressure that circles the continent between 60° and 70°S. In autumn, winds to the north of the low-pressure band slow the advancing ice edge. In summer, Ekman divergence created by opposing winds on either side of the low-pressure band opens up warm water regions that rapidly melt sea ice. We use the 40 ensemble members from the CESM-LENS historical run (1920–2005) to examine the relationship between the asymmetry in the annual cycle and the position and intensity of the low-pressure band. CESM-LENS reproduces the magnitude of the annual cycle of Antarctic sea ice extent with a short lag (2 weeks). Melt rate is the characteristic of the annual cycle that varies the most. Our results provide evidence that lower pressure leads to increased melt rates, which supports the importance of the role of divergence in increasing the melt rate of Antarctic sea ice. The role of winds during the growing season remains unquantified.

Introduction

Each year, the largest seasonal cycle in surface cover occurs in the Southern Ocean when sea ice grows from a minimum of less than 5 million square kilometers in February to a maximum of over 17 million square kilometers in September (Parkinson, 2019). Antarctic sea ice extent (SIE, the area of the ocean surface that contains sea ice exceeding some threshold value, usually 15%) has slightly increased over the 40-year satellite period, but in recent years, record high (2014) and record low (2017) SIEs have been observed. Due to the critical role played by sea-ice cover in our changing climate, the literature has been focused on examining the trends in Antarctic sea ice. However, a complete understanding of the mechanisms that drive the annual cycle may help to separate them from those that drive the observed interannual changes so that we might better understand the key processes driving trends in Antarctic sea ice, and consequently, global climate trends.

In each year of the satellite record, sea ice takes over 7 months to grow and less than 5 months to melt, with most of the melt occurring in just 3 months between November and January. Enomoto and Ohmura (1990) first linked this asymmetry to the semi-annual oscillation (SAO) of the circumpolar trough (CPT). The CPT is a band of low pressure that encircles Antarctica, occurring due to the net effect of the collective tracks of frequent individual storms (Jones and Simmonds, 1993; Turner and others, 1998). It is located between 60° and 70°S, and fluctuations in its strength and position are indicative of changes in a much larger system of cyclonic activity (Meehl, 1991). The SAO is a twice-yearly change in the intensity and location of the CPT in which it moves south and deepens in March and September/October, and moves north and weakens in June and December/January (Meehl, 1991; van Loon, 1967; Meehl and others, 1998; Raphael, 2004; Ackerley and Renwick, 2010). This oscillation is linked to differential cooling and heating rates between the Antarctic continent and the mid-latitude polar oceans (van Loon, 1967) and it affects many components of the Southern Hemisphere atmosphere and ocean. The resulting pattern can be depicted as a half-yearly wave in the sea level pressure difference between 50° and 65°S that explains more than 50% of the variability in the southern hemisphere sea level pressure (Raphael and Holland, 2006).

Enomoto and Ohmura (1990) were the first to describe a conceptual model to explain how the CPT drives the annual cycle of Antarctic sea ice. A key part of their model is that, despite considerable variations of both sea-ice extent and sea level pressure on a range of time and space scales, the ice edge crosses the CPT twice each year. The latitudinal range of the CPT is only 2° and it is the movement of the ice edge that primarily determines the location of the ice edge relative to the CPT. Westerly winds to the north of the CPT impart a northward Ekman component on sea-ice motion while easterlies to the south impart a southward component. Therefore, there is divergence of sea ice when the CPT overlies sea ice, or equivalently when the ice edge is to the north of the CPT. There can be convergence of sea ice when the ice edge is to the south of the CPT, depending on the north-south gradients in the winds. Convergence usually results in increased sea-ice concentration (SIC) locally but a lower SIE. However, the effect of divergence on SIE depends on the prevailing temperatures. In winter,
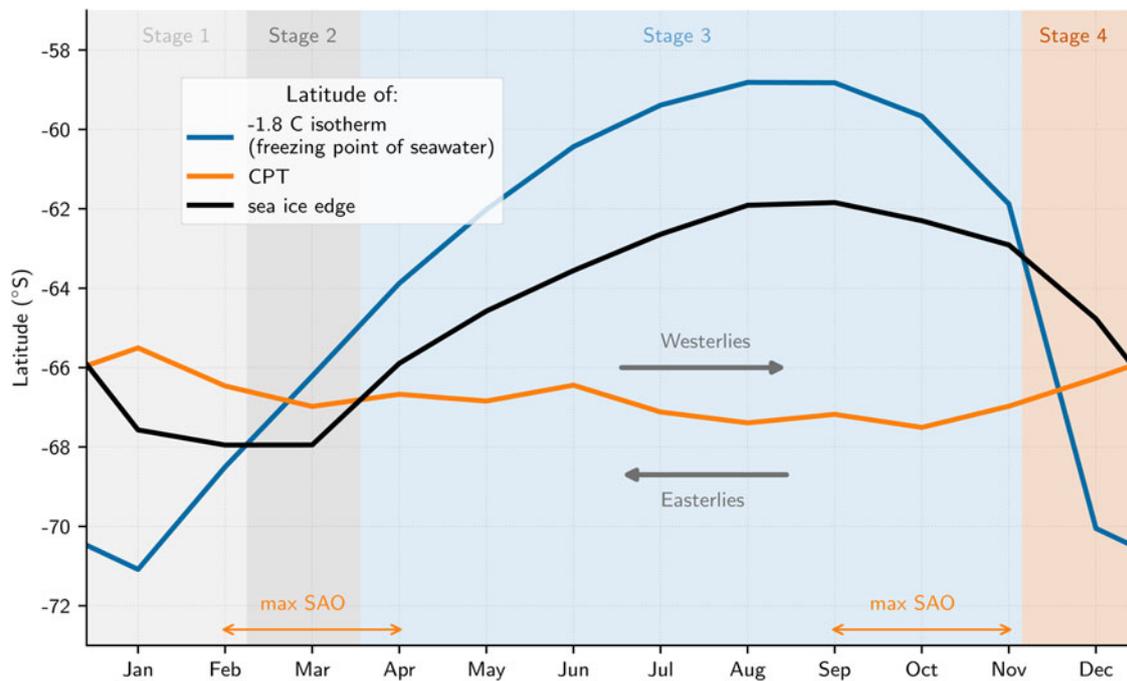
Fig. 1. Stages of the conceptual model of the processes driving the asymmetric annual cycle of Antarctic sea-ice extent. The blue line shows the monthly mean latitude of the freezing 2 m air temperature (− 1.8°C) from ERA-Interim and provides an indication of conditions for freezing/melting. The black line shows the monthly mean latitude of the ice edge, as calculated from the NOAA/NSIDC Climate Data Record. The orange line shows the monthly mean line of the CPT, as calculated from ERA-Interim monthly mean sea level pressure. Maximum SAO refers to times when the SAO causes the CPT to be most intense and contracted toward the continent. Modified from Eayrs and others (2019).

open water areas within the sea-ice field produce new ice, and the ice field expands northward (Gordon and Taylor, 1975), whereas after the spring equinox, increased heat absorption in these open water regions leads to rapid bottom and lateral melting (Maykut and Perovich, 1987), and consequent retreat of the ice edge. The conceptual model is summarized in Figure 1, which shows the monthly latitudes of SIE, the CPT and the freezing 2 m air temperature (− 1.8°C). Air temperature implies melting or freezing conditions. The combinations of convergence/divergence and melting/freezing conditions define four distinct stages in the annual cycle (Fig. 1):

- Stage 1: southward Ekman transport and melting conditions (mid Dec–early Feb)
- Stage 2: southward Ekman transport and freezing conditions (early Feb–mid Mar)
- Stage 3: divergence and freezing conditions (mid Mar–early Nov)
- Stage 4: divergence and melting conditions (early Nov–mid Dec)

During Stage 1 (Fig. 1, mid-December through early February), the ice edge is south of the CPT and conditions are warm enough for ice to melt. The ocean starts to freeze in late February (Stage 2), but the ice advance is hampered by southward Ekman transport associated with easterly winds. These winds are expected to play a dominant role during March when the CPT is at its most intense. In Stage 3, the ice edge advances north of the CPT and divergence opens up regions of the marginal ice zone that now freeze. However, the intensity of the CPT starts to weaken through this stage, and its influence continues to slow as the ice edge moves further away. The ice edge is considered to be in dynamic and thermal equilibrium at its maximum extent in September. During the latter part of Stage 3, the ice edge starts to retreat as any northward drift pushes the ice into warmer

regions where it now melts. Divergence creates areas of open water that now may not freeze in the warmer temperatures. The ice edge starts to retreat, moving closer to and eventually crossing the CPT in December (Stage 4). The resulting convergence contributes to a rapid retreat.

Enomoto and Ohmura (1990) initially described the role of the CPT in driving the asymmetric sea-ice cycle using low spatial and temporal datasets for 1982–1984. Eayrs and others (2019) demonstrated that this conceptual model holds for the full 40 years of the overlapping daily satellite and reanalysis record. However, the mechanism has not yet been quantified. In this analysis, we group model years from the CESM-LENS experiment with similar melt and growth behaviors and analyze the differences between these groups to examine the role of the CPT in driving asymmetry in the Antarctic sea-ice annual cycle. We find the largest differences to be in the melt rates and demonstrate that this is linked to divergence due to the presence of the CPT (Stage 4 of the conceptual model, Fig. 1). Our results show that the growth of Antarctic sea ice, the SAO index and the location of the CPT remain consistent across model years. Our analysis would have to be further refined to quantify the role of the winds during the growing season and identify the mechanisms that control the slow advance of Antarctic sea ice.

Data and Methods

CESM Large Ensemble project

Our analysis makes use of the 40 20th century (1920–2005) ensemble simulations performed with the Community Earth System Model Large Ensemble (CESM-LENS, Kay and others, 2015). CESM-LENS includes atmosphere (Community Atmosphere Model version 5, CAM5), ocean (Parallel Ocean Program, POP2), land (Community Land Model version 4, CLM4) and sea ice (Community Ice CodE version 4, CICE4) component models (Hurrell and others, 2013). All model components have ~1°

horizontal resolution; there are 60 vertical layers in the ocean and 30 in the atmosphere. All members of the ensemble are forced with identical historical forcing for 1920–2005 (Lamarque and others, 2010). The ensemble members differ only in a round-off level perturbation in their initial 1920 atmospheric state, and therefore any difference in their simulation is solely due to internal variability in the model. These outputs provide 3440 years of internal variability (40 ensembles × 86 years) in which we can examine how changes in the position and intensity of the CPT are related to the sea-ice annual cycle. Each of the historical ensemble runs shows a decreasing trend in SIE (Kay and others, 2015; Rosenblum and Eisenman, 2017) but we do not consider the distribution in time of each of the model years. We describe the model metrics for sea ice and atmosphere quantities in the relevant sections below. All model outputs are on a 365 d year.

Sea-ice metrics

Sea-ice metrics are derived from SIC. We downloaded daily and monthly mean SICs from the 25 km × 25 km NOAA/NSIDC Climate Data Record (CDR, Fetterer and others, 2017). The official version of the CDR only extends back to 1987, so in order to extend the record, we used the analogous 'Goddard merged' field, which is available from November 1978. The merged product in the CDR comprises the higher of the concentrations estimated by the Bootstrap algorithm (Comiso, 1986) and the NASA Team algorithm (Cavalieri and Parkinson, 2008), thereby overcoming the shortfalls in each method (Meier and others, 2014) – NASA Team is sensitive to snow layering and surface emissivity variations, while Bootstrap tends to underestimate concentrations in very low temperatures (Comiso and Steffen, 2001). Monthly and daily SIC (%) is available from the CICE4 model in CESM-LENS.

We describe the sea ice using daily SIE, maximum growth and melt rates, length (number of days) of growth and melt periods, and monthly mean latitude of the sea-ice edge. Daily SIEs were calculated from SIC by summing the areas of each pixel with a calculated SIC of at least 15%. The growth and melt rates were calculated by finding the gradient in SIE, i.e. the change in SIE per day. The number of days of growth (melt) is the number of days that the gradient in SIE is positive (negative). The mean latitude of the ice edge was calculated from the monthly datasets as the zonal mean latitude of the ice edge as defined by 15% SIC.

Atmospheric metrics

The mechanisms that drive the conceptual model are the location and intensity of the CPT and its SAO. These were derived from the mean sea level pressure from atmospheric reanalyses since meteorological observations are sparse in space and time across the Southern Ocean. We used ERA-Interim (Dee and others, 2011) and its successor, ERA5 (CDS, 2017), as this reanalysis set has been shown to have the best overall performance in high southern latitude (e.g. Bracegirdle and Marshall, 2012). Figure 1 was created using ERA-Interim and the rest of the analysis was conducted using ERA5. Mean sea level pressure (Pa) is available from the CAM5 model in CESM-LENS. We define the SAO index as the difference in mean sea level pressure between 50° and 65°S, following Meehl and others (1998). The monthly mean location of the CPT is the zonal mean latitude of the minimum pressure for each month.

Grouping of model years

There are two ways to define the differences in the growth and melt of sea ice:

(1) the ratio of the length of the growing season to the length of the melting season
(2) the ratio of the maximum melt rate to the maximum growth rate

We grouped the 3440 CESM-LENS model years using each of these methods to create combinations of years with similar sea-ice characteristics and then conducted an analysis of variance (ANOVA) to identify statistical differences between the groups. To address the pairwise comparison, we used the posthoc test of Tukey (Tukey procedure). As the criteria of significance, both methods use p-values, where values higher than 0.05 identify the groups are not statistically different. Once we had identified statistically different groups, we compared the intensity and location of the CPT across groups to investigate the role of the CPT on the annual cycle of SIE.

Results

Model performance

We compared the mean annual cycles during the overlapping period between the model and satellite and reanalysis datasets (1979–2005) to confirm that the CESM-LENS outputs adequately capture the seasonal cycle in Antarctic SIE and the changes in the CPT that are understood to drive this cycle. The model performance compared to the satellite and reanalysis datasets is summarized in Figure 2. The CESM-LENS ensemble mean minimum in SIE is slightly higher than the mean satellite annual cycle and the maximum is slightly less, suggesting that, on average, the CESM-LENS runs do not quite melt enough ice in the summer or grow quite enough ice in the winter (Table 1 and Fig. 2a). However, the differences are less than 0.5 million square kilometers, which is less than the variability in SIE between different satellite products (Meier and Stewart, 2019) and overall, unlike many other climate models (e.g. Turner and others, 2013), CESM-LENS correctly reproduces the amplitude of the Antarctic seasonal cycle. The ensemble mean has an even more sluggish turn at the maximum than that observed by satellite, with sea ice at more than 99% of its maximum for a week longer than in the satellite data (33 days compared to 27 days, Table 1). However, both the model and observed SIE are at a minimum period for 18 days. We define the minimum period as the number of days when the SIE was in the lowest 1% of its annual range. There is a timing mismatch between the ensemble mean and observed mean: minimum SIE occurs 2 weeks late in the ensemble mean, in March rather than February. Similarly, the maximum SIE is 9 days late, although for both CESM-LENS and the satellite, this occurs in September. The annual cycle in the ensemble mean is asymmetric, but the time from minimum to maximum is 5 days shorter than in the satellite dataset.

The maximum growth and melt rates are also well-represented by the model, with the ensemble-mean maximum melt rate modeled as approximately double the growth rate and very similar in magnitude to the satellite rates (Fig. 2b). The distributions of melt and growth rates in the CESM-LENS model years match well with the distributions in the satellite observations (Fig. 3), but the maximum growth and melt rates are slightly weaker in the CESM-LENS outputs. However, this difference is only about 20 000 km^2 per day (filled squares in Fig. 3), which is indistinguishable from the standard deviations in the CESM-LENS outputs (±50 000 km^2 per day for the growth rates and ±20 000 km^2 per day for the melt rates). This matches the fact that the SIE is slightly too high in summer and slightly too low in winter (Fig. 2a). The variability in melt and growth rates is the same for the model and the satellite datasets (horizontal lines in Fig. 3), but the standard
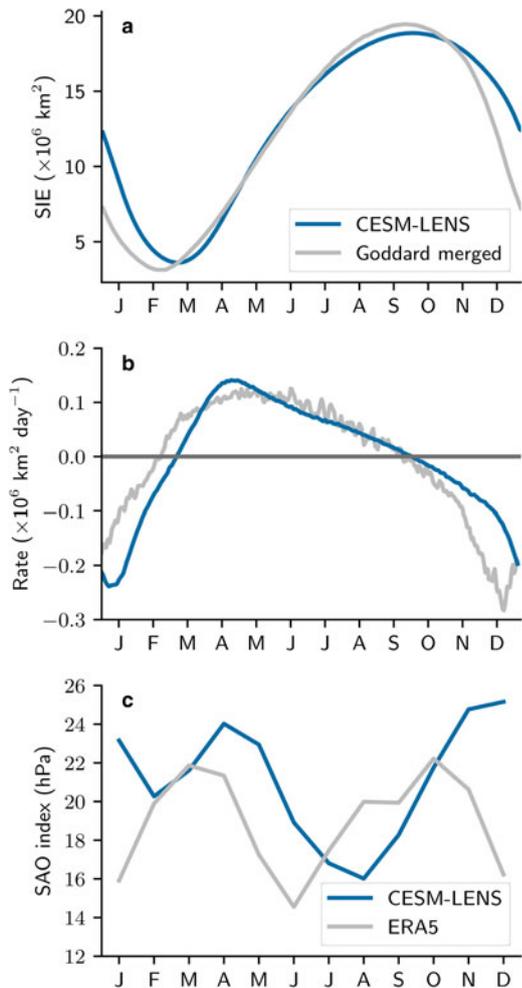
Fig. 2. (a) Comparison of ensemble mean daily SIE (CESM-LENS, blue) with the Goddard merged satellite product (gray line) for the overlapping period (1979–2005). (b) Rate of daily ice growth (positive values) and ice melt (negative values) for the SIEs in (a). (c) Mean monthly 1979–2005 SAO index for mean sea level pressure (CESM-LENS = blue; ERA5 = gray line).

Table 1. Statistics for the mean SIE averaged over 1979–2005 (overlapping period)

	CESM-LENS	Satellite
Min (10^6 km^2)	3.6	3.1
Max (10^6 km^2)	18.9	19.5
Min (day of year)	67	53
Max (day of year)	272	263
Growth days	205	214
Melt days	161	152
Days at min	18	18
Days at max	33	27
Max growth rate (day of year)	117	126
Max melt rate (day of year)	15	351
Max growth rate (10^6 km^2 d^{-1})	0.14	0.12
Max melt rate (10^6 km^2 d^{-1})	− 0.21	− 0.23

deviation in the maximum melt rate more than three times that in the growth rate, illustrating an asymmetry not only in the rates but also in the interannual variability of the rates.

The seasonal cycle of sea-ice growth in the CESM-LENS ensemble mean is slightly different from the mean cycle derived from satellite observations. In particular, the CESM-LENS growth rate peaks quite sharply in April, whereas the observed peak growth rate is maintained over April/May/June (Fig. 2b). The
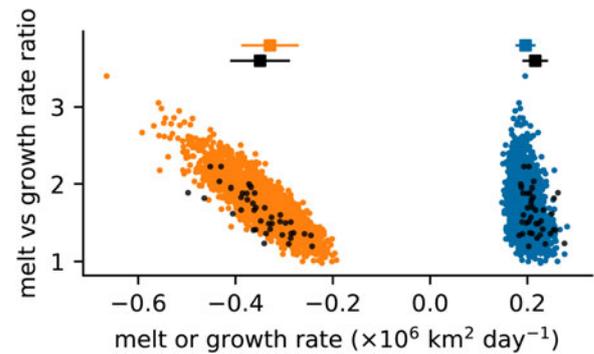
Fig. 3. Scatter plot of the maximum growth rate (blue dots) and melt rate (orange dots) with the ratio of maximum melt rate to maximum growth rate ('melt vs growth rate ratio' on the y-axis). The black dots show the same information from the satellite observations. The filled squares at the top show the mean values with their standard deviations (horizontal lines).

Table 2. Mean SAO index averaged over 1979–2005 (overlapping period)

Description	CESM-LENS		ERA5	
	Month	SAO index (Pa)	Month	SAO index (Pa)
Spring maximum	Dec	25.2	Oct	22.2
Winter minimum	Aug	16.0	Jun	14.6
Autumn maximum	Apr	24.0	Mar	21.9
Summer minimum	Feb	20.3	Jan	15.9

model ensemble mean starts melting at about the same time as the satellite mean (late September), but the CESM-LENS melt rate is much slower than in the satellite dataset for the first few months of the melting season. Peak melt rate is about 3 weeks late in the model ensemble mean – in January rather than December – and is very slightly weaker. One consequence of these differences is that the time between the maximum melt rate and the maximum growth rate is longer in the model.

We used the monthly rather than the daily SAO index since the daily index has a large amount of noise due to the effect of storms. Storms will be important to consider at the local scale as they have been shown to have a significant impact on the marginal ice zone (Vichi and others, 2019), but here we consider the monthly pressure fields. The modeled SAO index has a similar timing issue to the SIE (Fig. 2c). The first oscillation is about a month late, with the minimum (summer minimum) in February instead of January and the maximum (autumn maximum) in April instead of March (Table 2). The second oscillation lags even further behind the ERA5 mean; the minimum (winter minimum) is in August rather than June, and the maximum (spring maximum) is in December instead of October. The intensity of the SAO index is larger in the CESM-LENS ensemble mean, with maxima 2–3 Pa higher than in the ERA5 reanalyses. CESM-LENS does not produce the summer minimum seen in the ERA5 reanalyses, and the summer pressure difference between the mid-latitude and the polar regions is 5 Pa higher than in the ERA5 reanalyses. However, the SAO in mean sea level pressure is evident in the CESM-LENS outputs.

We consider the annual cycles of SIE (cross-correlation of 0.91) and the SAO (cross-correlation of 0.71) to be sufficiently well-reproduced in CESM-LENS to use the historical ensembles to examine the role of the changes in the CPT in driving the annual cycle of Antarctic sea ice. It is interesting to note that both the modeled annual cycle of SIE and the modeled SAO index have a lag compared to the observations. The lag is

3 weeks in the SIE, with the CESM-LENS mean 1979–2005 annual cycle of SIE shifted by 22 days compared to the mean annual cycle for the Goddard merged product (Fig. 2a). The lag is even larger in the SAO (Fig. 2c) and increases for the spring peak. The mean 1979–2005 CESM-LENS SAO index autumn peak is a month later than the mean 1979–2005 ERA5 autumn peak; the mean 1979–2005 CESM-LENS SAO index spring peak is 2 months later than the mean 1979–2005 ERA5 spring peak. Note that the SAO is shown in the monthly mean pressure data rather than the daily mean, these lags are measured on different time scales. Overall, the CESM-LENS outputs provide a useful tool to examine the role of the CPT in driving asymmetry in the seasonal cycle of SIE.

Analysis of different patterns of SIE

Our model did not show any statistical difference between groups when classifying by the number of days of growing vs melting (ANOVA analysis with p-values >0.05), so we present here only the groups that were split according to the max growth and melt rates. We discuss later some of the difficulties related to defining the annual cycle by the length of the growing and melting seasons in each year. The groups are named according to the ratio of the melt rate to the growth rate so that the group with a melt rate equal to the growth rate is called Melt 1.0x Growth, the group with a melt rate 1.5 times the growth rate is called Melt 1.5x Growth, and so on.

The distribution of annual cycles of SIE into groups by the ratio of their maximum melt to their maximum growth rates is similar between the 40 satellite years and the 3440 model years (Fig. 4). Note that this distribution does not change when we compare the groups for only the overlapping period (1979–2005). In each case, nearly 60% have a ratio of 1.5, i.e. a maximum melt rate 1.5 times larger than the maximum growth rate, and about a third have a maximum melt rate twice the maximum growth rate. The inset in Figure 4a shows that there is no discernible trend in the observed ratio, although the growth rates are lower in the late 1990s/early 2000s and seem to be recovering by 2005.

The ANOVA test returned a p-value <0.05 showing that Melt 1.0x Growth, Melt 1.5x Growth and Melt 2.0x Growth are statistically different. Table 3 shows the Tukey statistical comparisons between groups. The first two columns show the groups that are compared. The third column shows spread of values in each group (sum of squares, SS), the fourth column has the degree of freedom (df) associated with the estimated group means and the fifth column gives the mean squares (MS, the ratio SS/df).
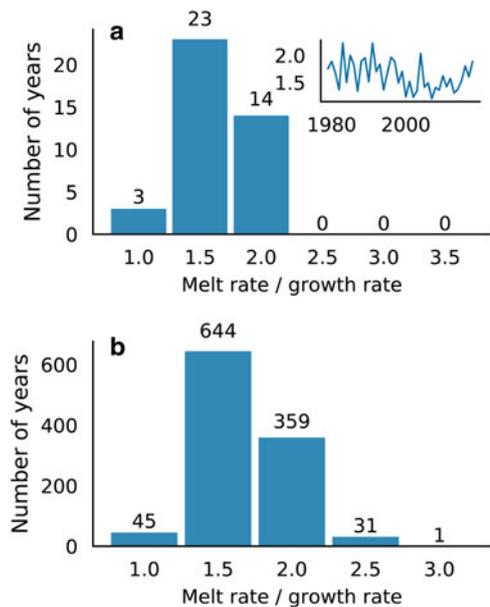
Fig. 4. Grouping of the 3440 model years according to the ratio between the maximum sea-ice melt rate and the maximum sea-ice growth rate. (a) 40 years from satellite observations (1979–2018); (b) 3440 years from CESM-LENS. The inset in (a) is a time series of the ratio between the maximum sea-ice melt rate and the maximum sea-ice growth rate.

The F-statistic in the sixth column is the ratio of the mean squares. The last column lists the level at which the Tukey p-value meets the significance criteria. The difference of Melt 1.0x Growth is statistically highly significant ($p < 0.001$) to Melt 1.5x Growth, Melt 2.0x Growth and Melt 2.5x Growth. Melt 1.5x Growth is statistically highly different ($p < 0.001$) to Melt 2.0x Growth. We removed Melt 2.5x Growth, which is only statistically different to Melt 1.0x Growth, and Melt 3.0x Growth and Melt 3.5x Growth, as they are not statistically different to any of the other groups.

Figure 5a shows the rate of change in SIE for each of the groups used in the analysis (Melt 1.0x Growth, Melt 1.5x Growth and Melt 2.0x Growth). There is high interannual variability in the rate of change of SIE for all of the groups (Fig. 5b). There is a very slight decrease in maximum growth rate between groups (Table 4, variation of up to 20 000 km^2 per day) but a large change in the melt rates, with Melt 2.0x Growth melting 130 000 km^2 per day more ice than Melt 1.0x Growth (Table 5). In fact, most of the variation between the groups is due to the change in melt rate and there is very little

Table 3. ANOVA test of significance between groups

GroupxGroup		SS	df	MS	*F*	*p*-value
Melt 1.0x Growth	Melt 1.5x Growth	14115.81	18622.82	23129.83	2.07E-08	$p < 0.001$
Melt 1.0x Growth	Melt 2.0x Growth	18962.42	23595.64	28228.86	2.07E-08	$p < 0.001$
Melt 1.0x Growth	Melt 2.5x Growth	13886.39	20132.68	26378.96	2.07E-08	$p < 0.001$
Melt 1.0x Growth	Melt 3.0x Growth	832.69	17032.21	33231.73	0.033	$p < 0.05$
Melt 1.0x Growth	Melt 3.5x Growth	− 54314.64	− 77.49	54159.66	0.99	–
Melt 1.5x Growth	Melt 2.0x Growth	2956.34	4972.81	6989.29	2.07E-08	$p < 0.001$
Melt 1.5x Growth	Melt 2.5x Growth	− 3139.39	1509.86	6159.11	0.94	–
Melt 1.5x Growth	Melt 3.0x Growth	− 17243.85	− 1590.61	14062.63	0.99	–
Melt 1.5x Growth	Melt 3.5x Growth	− 72776.81	− 18700.31	35376.19	0.92	–
Melt 2.0x Growth	Melt 2.5x Growth	− 8234.66	− 3462.96	1308.74	0.30	–
Melt 2.0x Growth	Melt 3.0x Growth	− 22253.47	− 6563.43	9126.62	0.84	–
Melt 2.0x Growth	Melt 3.5x Growth	− 77760.29	23673.12	30414.04	0.81	–
Melt 2.5x Growth	Melt 3.0x Growth	− 19340.14	3100.47	13139.2	0.99	–
Melt 2.5x Growth	Melt 3.5x Growth	− 74459.32	20210.17	34038.99	0.90	–
Melt 3.0x Growth	Melt 3.5x Growth	− 73380.29	− 17109.70	39160.89	0.95	–

SS, sum of squares; df, degrees of freedom; MS, mean squares which is the ratio SS/df; *F*, ratio of the mean squares (*F*-statistic)
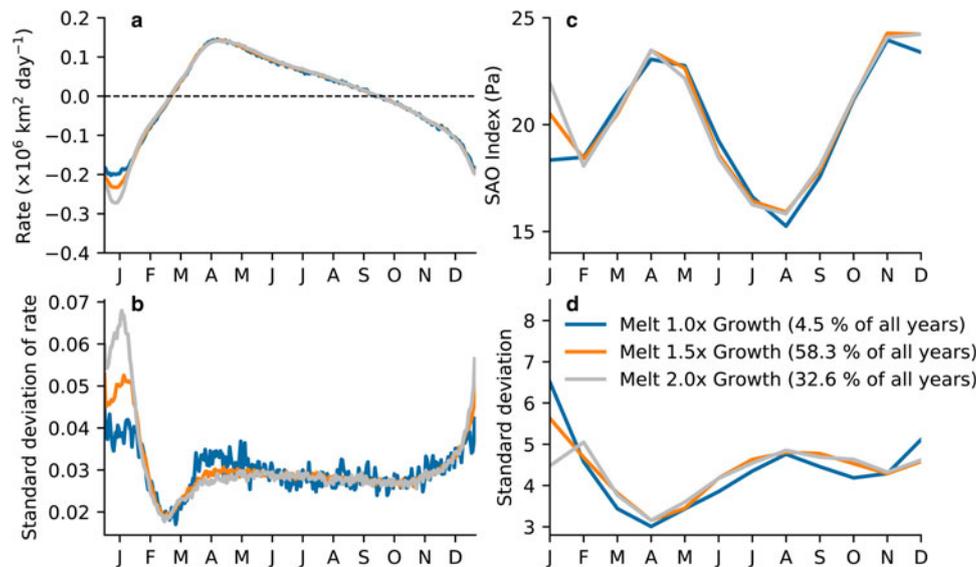
Fig. 5. (a) Mean rate of change in SIE for each group. (b) Standard deviation of the rate of change in SIE for each group. (c) Mean SAO index for each of the groups. (d) Standard deviation of the rate of change in SAO for each group.

Table 4. Statistics for the growth rate of SIE (10^6 km^2 d^{-1}) for each of the groups

Group	Max	Mean	Day
Melt 1.0x Growth	0.28	0.21 (±0.02)	119 (±15)
Melt 1.5x Growth	0.28	0.20 (±0.02)	120 (±14)
Melt 2.0x Growth	0.25	0.19 (±0.02)	121 (±15)

'Day' gives the day of the year of the average maximum growth rate for each group. The numbers in brackets are the mean standard deviations; 'Max' is the maximum value for each group; 'Mean' is the mean value for each group.

Table 5. Statistics for melt rate of SIE (10^6 km^2 d^{-1}) for each of the groups

Group	Max	Mean	Day
Melt 1.0x Growth	− 0.31	− 0.25 (±0.03)	9 (±9)
Melt 1.5x Growth	− 0.43	− 0.30 (±0.03)	10 (±8)
Melt 2.0x Growth	− 0.55	− 0.38 (±0.04)	11 (±6)

'Day' gives the day of the year of the average maximum melt rate for each group. The numbers in brackets are standard deviations; 'Max' is the maximum melt rate for each group (i.e. the minimum growth rate); 'Mean' is the mean value for each group.

change in growth rate (Fig. 5a). Conversely, there is considerable variation in the timing of the maximum growth rate with the standard deviation of the order of 2–3 weeks (Table 4) but the standard deviation in the timing of the maximum melt rate is less than 10 days for each of the groups (Table 5). Even though the value of the melt rate changes considerably between groups, the timing of the maximum melt rate remains consistent, changing on the order of days, increasing from day 9 in Melt 1.0x Growth to day 11 in Melt 2.0x Growth.

There is not a straightforward relationship between the intensity of the SAO index and the different groups (Fig. 5c). For the most part, the seasonal cycle of the SAO index is very similar between the groups (Fig. 5c), but there is considerable variation between years (Fig. 5d). Note that the standard deviations of the SAO indices are very large compared to the difference between groups (Fig. 5d) whereas in the annual cycle of the rate of change of SIE, even the maximum standard deviations, which coincide with the maximum melt rate, are much smaller than the difference between groups (Fig. 5b).

The two key parts of the conceptual model are Stage 2, when the advancing ice edge is slowed by Ekman transport associated with easterly winds, and Stage 4, when divergence creates open water areas that lead to rapid melting (Fig. 1). There are some timing differences in the stages of the CESM-LENS outputs comparing Figure 1 to Figure 6. This is partly due to the lag in the timing of the SIE and CPT in the CESM-LENS outputs, as discussed earlier (Fig. 2). However, one significant difference in the stages is caused by the fact that during December and January, the freezing isotherm in the model is further north than in the reanalyses. We might expect the latitude of the freezing temperature to be 9° further south in December and 8° further south in January. This results in a very brief Stage 1 (1 week compared to approximately a month and a half). We suspect that the boundary between Stage 1 and Stage 2 should occur during March. The standard deviation of the latitude of the ice edge is 0.5°, which is similar to the difference in latitude of the ice edge between the group means. The standard deviation of the latitude of the CPT is 1.5°, which is larger than the difference between the group means. However, since our groups are statistically distinct, we compare the differences between the group mean latitudes of sea-ice edge, CPT and freezing isotherm, following the stages of the conceptual model.

Melting (Stage 4 and Stage 1) In January (Stage 4), there is a higher SAO index for a higher melt rate to growth rate (Fig. 5c). This coincides with the timing of the maximum melt rate (Figs 5a and 7b), which supports the theory that the divergence caused by the CPT in spring aids faster melting of the sea ice. Proximity to the ice edge is not important at this time since the role of the CPT is to open up the ice pack to allow the ice-ocean albedo feedback, the areal albedo change due to variations in the open water fraction (Nihashi and Ohshima, 2001; Nihashi and Cavalieri, 2006), to increase the rate of melting. The timing of the maximum melt rate is consistent (Fig. 7b, day 10 for all groups with a standard deviation of 7 days). There are no significant differences between the groups during the very brief Stage 1, the part of the cycle when southward Ekman transport aids the retreat of sea ice.

Growing (Stage 2 and Stage 3) Stage 2 is the period in the conceptual model when easterly winds slow the sea-ice advance. We do not find any significant differences in the growth rates (Fig. 5a), the magnitude of the SAO index (Fig. 5c) or the
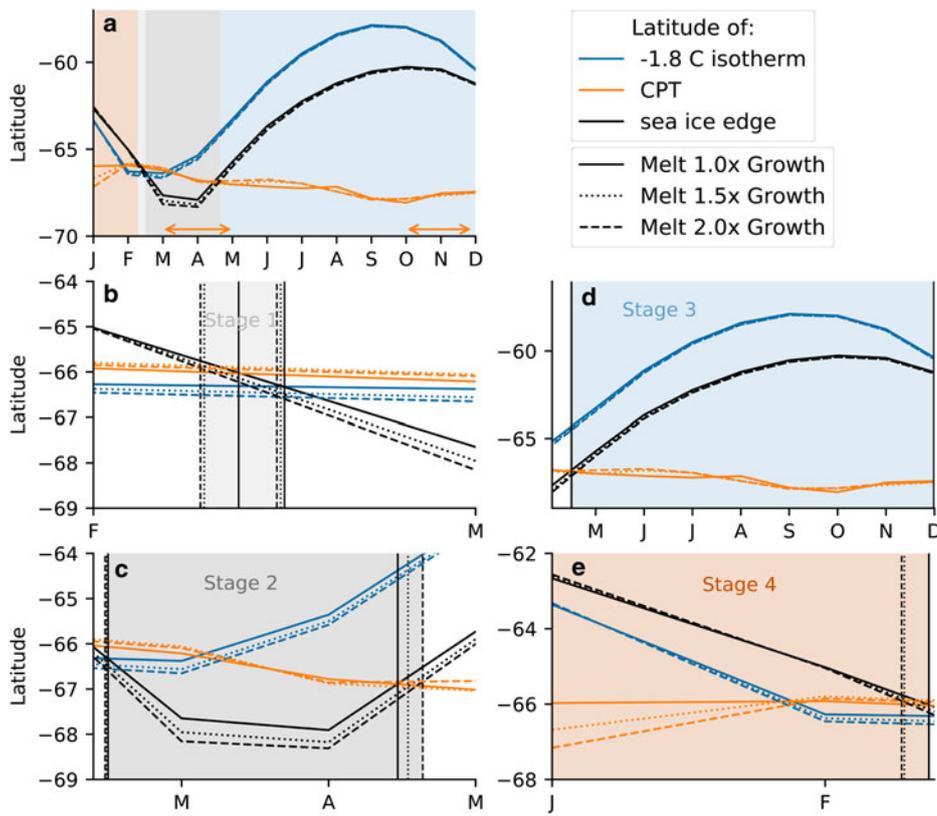
Fig. 6. (a) Conceptual model for the mean of the three cluster groups (Melt 1.0x Growth has solid lines; Melt 1.5x Growth has dotted lines; Melt 2.0x Growth has dashed lines). The horizontal arrows indicate when the SAO is maximum. The shading identifies each of the stages in the conceptual model (Stage 1 – light gray; Stage 2 – dark gray; Stage 3 – blue; Stage 4 – orange). (b)–(e) are zoomed-in versions of (a). (b) Stage 1 of the conceptual model (melting and convergence, light gray). (c) Stage 2 (freezing and convergence, dark gray). (d) Stage 3 (freezing and divergence, blue). (e) Stage 4 (melting and divergence, orange). The differences in the start and end time of each stage are shown by the vertical solid lines (Melt 1.0x Growth), the vertical dotted lines (Melt 1.5x Growth) and the vertical dashed lines (Melt 2.0x Growth).
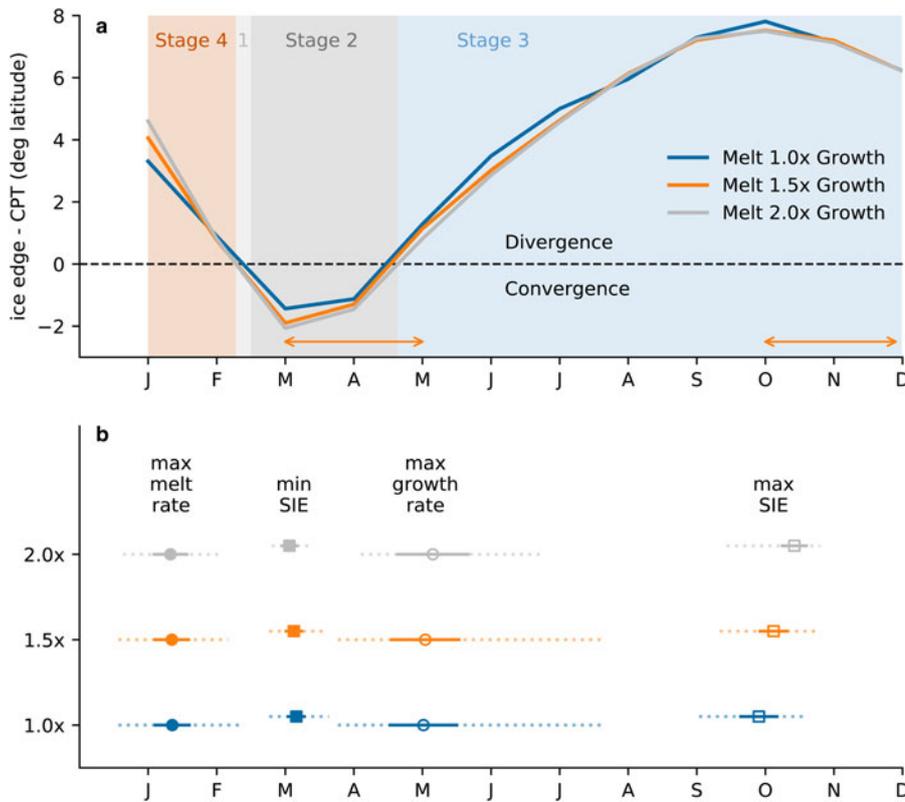
Fig. 7. (a) Distance between the sea-ice edge and the location of the CPT for each of the model groupings. Horizontal orange arrows indicate the times when the SAO is maximum. Shading indicates the different stages of the conceptual model: Stage 1 (light gray), Stage 2 (dark gray), Stage 3 (blue), Stage 4 (orange). (b) Timing of the maximum melt rates (filled circles), maximum growth rates (open circles), minimum SIEs (filled squares) and maximum SIEs (open squares) for each group. Horizontal lines show the range of values in each group (solid lines = standard deviations; maximum range = dotted lines). The squares are slightly offset from the circles to aid readability.

location of the CPT (Fig. 6c) during this stage. Stage 2 ends when the ice edge moves equatorward of the CPT. Stage 2 ends later for increasing melt to growth ratio, but the differences in timing between the group means are within the standard deviations (vertical solid line, vertical dotted line and vertical dashed line in Fig. 6c). The maximum growth rates occur at the beginning of Stage 3, just after the ice edge

moves north of the CPT (Fig. 7). The timing of maximum growth rate is also later for increasing melt to growth ratio, but differences in timing between the group means are small compared to the standard deviations (Fig. 7b, open circles). Maximum SIE is notably later for Melt 2.0x Growth, but this does not appear to be related to the timing (Fig. 7b) or intensity (Fig. 5d) of the CPT.

Discussion

This work builds on the work of Enomoto and Ohmura (1990), who first suggested the role of the SAO of the CPT in modulating the annual cycle of Antarctic sea ice. This mechanism has not yet been quantified, and our understanding of the mechanisms that drive the asymmetric annual cycle of Antarctic sea ice is limited by the lack of a long homogeneous record of SIE, concentration and thickness. Furthermore, observations of the surrounding ocean are geographically sparse and temporally short, and there are almost no atmospheric measurements over the sea-ice zone (e.g. Hobbs and others, 2016). Given these shortcomings, we use climate model outputs to analyze the role of the CPT in driving the asymmetry in the annual cycle of SIE.

Although the Coupled Model Intercomparison Project (CMIP) models show considerable deficiencies in capturing the full magnitude of the annual cycle of Antarctic sea ice, they do tend to capture its asymmetric pattern and timing (Eayrs and others, 2019), suggesting that the mechanisms driving the asymmetric cycle are already included in climate models. The complexity of the sea-ice components in these models varies substantially (Roach and others, 2018) and assessing these mechanisms across the CMIP models is complicated by the need to take into consideration the differences in the model physics. Therefore, we chose to use the 40 ensemble members of the 86-year historical CESM-LENS so that we could investigate the variability of the annual cycle for a large number of model years, without having to account for differences in model physics.

Several studies have examined the trends and variability of Arctic sea ice in CESM-LENS (Swart and others, 2015; Barnhart and others, 2016) but, as far as we are aware, this is the first study to assess the ability of CESM-LENS to reproduce the annual cycle of Antarctic sea ice and aspects of the surface pressure field relevant to the representation of the CPT. CESM-LENS realistically reproduces the seasonal cycle of Antarctic SIE, albeit with a 3-week time lag. The model performs well in terms of minimum and maximum SIE, and minimum and maximum rates of change. There is a strong cross-correlation with the mean annual cycle in the satellite data. The 3-week timing offset (delay) in the annual cycle may be due to a delay in the timing of the SAO. The magnitude of the SAO index is larger in the CESM-LENS compared to the ERA5 reanalyses (Fig. 2c), but with the lack of observations of sea level pressure in the Southern Ocean, it is difficult to assess whether this is due to an overestimation in the model or an underestimation in the reanalyses. Given the Antarctic sea-ice zone is almost entirely devoid of conventional meteorological observations (Jonassen and others, 2019), assessments of the performance of the reanalysis datasets in the Southern Ocean are primarily based on data collected at weather stations on the continent. The bias in reanalysis pressure fields from these studies is 2–3 Pa (Bracegirdle and Marshall, 2012; Bromwich and others, 2013), which is similar to the difference in the SAO index between CESM-LENS and ERA5. Overall, CESM-LENS reproduces the annual cycles of SIE and the SAO sufficiently well for the purposes of this study.

Melt rate is the characteristic of the annual cycle that varies the most between model years; the growth rate remains surprisingly consistent. Our analysis assembled different annual cycles of SIE into groups with similar melt rates. We showed that higher January melt rates coincided with higher January values in the SAO index. Higher values in the SAO index imply a deeper CPT, increased winds and a larger associated Ekman transport. At this time, the CPT is located to the south of the ice edge and the opposing easterlies and westerlies open up regions of warmer water that help to rapidly melt the ice through the ice-ocean albedo effect (Stage 4). Melt 2.0x Growth had the highest January SAO index and Melt 1.0x Growth, the group with almost equal melt and growth rates, had particularly low values of the SAO index during this time (Fig. 5c).

It is important to consider some of the limitations of this study:

(1) SIE and SIC are incomplete descriptors of the sea-ice state, and lower SIE does not necessarily equate to thinner sea ice or lower ice volume. For example, sea-ice thicknesses of 20 m resulting from extreme ice compaction by strong and persistent northwesterly winds coincided with a period of anomalously low regional SIE in the Bellingshausen Sea in October 2001 (Massom and others, 2006). A consideration of seasonal changes in sea-ice volume is needed to provide a full description of the annual cycle of Antarctic sea ice. Research is ongoing to quantify Antarctic sea-ice thickness and its seasonal and inter-annual changes. As discussed by Roach and others (2018), SIE does not take into account any sub-grid scale sea-ice information and model simulations with the same SIE could have very different sea-ice cover characteristics. The distribution of SIE is controlled by local production (melting and freezing) and advection, but advection plays a greater role in regions of low SIC (Hibler, 1986). For now, we use the existing, robust observations of SIE to study the annual cycle but ultimately there is a need for additional information on sea-ice thickness and volume.

(2) Mean fields only provide an indication of low-level atmospheric structure; considerable longitudinal variation is lost in the averaging. The sub-Antarctic region is host to energetic and frequent cyclonic systems (Vichi and others, 2019). By using the monthly mean pressure, we ignore the considerable role that these storms play in shaping the local ice edge. The regularity of the pattern of the Antarctic sea-ice annual cycle suggests that although storms are important at the local scale, individually, they do not play a significant role in the asymmetry of the annual cycle. In terms of longitudinal variability, this analysis does not consider the significant spatial heterogeneity in SIE (Raphael and Hobbs, 2014). It may be that different mechanisms control the growth and melt of sea ice in different regions around Antarctica.

(3) In order to investigate the processes in the conceptual model, we need to interpret the variability in the daily rate of change of SIE in terms of dynamic changes at the ice edge. However, many other transient processes, such as cloud cover, can affect the daily rate of change of SIE. Such variability makes it difficult to accurately define the times of maximum growth and melt rates.

(4) The length of the annual cycle is affected by the timing of the maximum and minimum SIE, but if both are early (or late), the length of the growing and melting seasons will not change. We suspect that this complication in defining the length of the growing and melting seasons explains why we were unable to produce statistically different model year groups when classifying by the number of days of growing vs melting.

Conclusions

We explored the relationship between the low-pressure band around Antarctica and the seasonal cycle of SIE using the historical CESM-LENS ensembles. CESM-LENS reproduces well the pattern and timing of the Antarctic sea-ice annual cycle, and these outputs are therefore a useful tool to explore this relationship. We compared the changes in strength and location of the

CPT for different ratios of maximum melt rate to maximum growth rate. On average, the annual cycle of Antarctic SIE is a consistent signal and we were unable to separate the model outputs into groups with statistically different means. However, we were able to allocate groups by differences in the ratio of their melt and growth rates. Surprisingly, the magnitude of the growth rate does not vary significantly, but there are large variations in the magnitude of the melt rate. Our method does not quantify the role of the CPT during the growing period (Stages 2 and 3 of the conceptual model). We found a relationship between the spring maximum SAO index and the melt rate, which supports the theory that divergence in spring (Stage 4) opens up warmer water regions that help to melt the ice faster through the ice-ocean albedo effect.

The asymmetric cycle in Antarctic sea ice is an interesting phenomenon because its regularity stands in stark contrast to the large inter-annual variability in the mechanisms that are understood to drive it, especially since this cycle is the largest annual change in surface cover on the planet. Climate models provide an important tool for interpreting Antarctic sea-ice observations, but until we can understand the processes that drive the annual cycle and adequately model them, we are limited in our ability to model future changes and understand the processes that drive them. This work contributes an important part of ultimately reaching that global understanding.

References

CDS (2017) ERA5: Fifth generation of ECMWF atmospheric reanalyses of the global climate. Copernicus Climate Change Service Climate Data Store (CDS).

Ackerley D and Renwick JA (2010) The Southern Hemisphere semiannual oscillation and circulation variability during the Mid-Holocene. *Climate of the Past* 6(4), 415–430. doi: 10.5194/cp-6-415-2010

Barnhart KR, Miller CR, Overeem I and Kay JE (2016) Mapping the future expansion of Arctic open water. *Nature Climate Change* 6(3), 280–285.

Bracegirdle TJ and Marshall GJ (2012) The reliability of Antarctic tropospheric pressure and temperature in the latest global reanalyses. *Journal of Climate* 25(20), 7138–7146. doi: 10.1175/JCLI-D-11-00685.1

Bromwich DH, Otieno FO, Hines KM, Manning KW and Shilo E (2013) Comprehensive evaluation of polar weather research and forecasting model performance in the Antarctic. *Journal of Geophysical Research Atmospheres* 118(2), 274–292. doi: 10.1029/2012JD018139

Cavalieri D and Parkinson CL (2008) Antarctic sea ice variability and trends, 1979–2006. *Journal of Geophysical Research: Oceans* 113(C7), C07003. doi: 10.1029/2007JC004564.

Comiso JC (1986) Characteristics of Arctic winter sea ice from satellite multispectral microwave observations. *Journal of Geophysical Research: Oceans* 91(C1), 975–994. doi: 10.1029/JC091iC01p00975

Comiso JC and Steffen K (2001) Studies of Antarctic sea ice concentrations from satellite data and their applications. *Journal of Geophysical Research: Oceans* 106(C12), 31361–31385. doi: 10.1029/2001jc000823

Dee D and 18 others (2011) The ERA-Interim reanalysis: configuration and performance of the data assimilation system. *Quarterly Journal of the Royal Meteorological Society* 137(656), 553–597. doi: 10.1002/qj.828

Eayrs C and 6 others (2019) Understanding the seasonal cycle of Antarctic sea ice extent in the context of longer-term variability. *Review of Geophysics* 95, 1037–1064. doi: 10.1029/2018RG000631.

Enomoto H and Ohmura A (1990) The influences of atmospheric half-yearly cycle on the sea ice extent in the Antarctic. *Journal of Geophysical Research* 95(C6), 9497–9511. doi: 10.1029/JC095iC06p09497

Fetterer F, Savoie M, Mallory S, Duerr R and Stroeve J (2017) NOAA/NSIDC Climate Data Record of Passive Microwave Sea Ice Concentration, Version 3 [Antarctica] (doi: 10.7265/N59P2ZTG.), [Date accessed: 16 January, 2018].

Gordon A and Taylor H (1975) Seasonal change of Antarctic sea ice cover. *Science (New York, NY)* 187(4174), 346–347. doi: 10.1126/science.187.4174.346

Hibler W (1986) Ice dynamics. In Untersteiner N (ed.), *The Geophysics of Sea Ice*. Boston, MA: Springer, pp. 577–640, chapter 9.

Hobbs W and 5 others (2016) A review of recent changes in Southern Ocean sea ice, their drivers and forcings. *Global and Planetary Change* 143, 228–250. doi: 10.1016/j.gloplacha.2016.06.008

Hurrell JW and 22 others (2013) The Community Earth System Model: a framework for collaborative research. *Bulletin of the American Meteorological Society* 94(9), 1339–1360. doi: 10.1175/BAMS-D-12-00121.1

Jonassen MO and 5 others (2019) Assessment of atmospheric reanalyses with independent observations in the Weddell Sea, the Antarctic. *Journal of Geophysical Research: Atmospheres* 124(23), 12468–12484. doi: 10.1029/2019JD030897

Jones D and Simmonds I (1993) A climatology of Southern-Hemisphere extratropical cyclones. *Climate Dynamics* 9(3), 131–145. doi: 10.1007/BF00209750

Kay JE and 20 others (2015) The community earth system model (CESM) large ensemble project: a community resource for studying climate change in the presence of internal climate variability. *Bulletin of the American Meteorological Society* 96(8), 1333–1349. doi: 10.1175/BAMS-D-13-00255.1.

Lamarque JF and 21 others (2010) Historical (1850–2000) gridded anthropogenic and biomass burning emissions of reactive gases and aerosols: methodology and application. *Atmospheric Chemistry and Physics* 10(15), 7017–7039. doi: 10.5194/acp-10-7017-2010

Massom RA and 12 others (2006) Extreme anomalous atmospheric circulation in the West Antarctic Peninsula region in austral spring and summer 2001/02, and its profound impact on sea ice and biota. *Journal of Climate* 19(15), 3544–3571.

Maykut G and Perovich D (1987) The role of shortwave radiation in the summer decay of a sea ice cover. *Journal of Geophysical Research: Oceans* 92(C7), 7032–7044. doi: 10.1029/JC092iC07p07032

Meehl GA (1991) A reexamination of the mechanism of the semiannual oscillation in the Southern Hemisphere. *Journal of Climate* 4(9), 911–926. doi: 10.1175/1520-0442(1991)004<0911:AROTMO>2.0.CO;2

Meehl GA, Hurrell J and van Loon H (1998) A modulation of the mechanism of the semiannual oscillation in the Southern Hemisphere. *Tellus, Series A: Dynamic Meteorology and Oceanography* 50(4), 442–450. doi: 10.3402/tellusa.v50i4.14537

Meier WN, Peng G, Scott DJ and Savoie MH (2014) Verification of a new NOAA/NSIDC passive microwave sea-ice concentration climate record. *Polar Research* 33(1), 21004. doi: 10.3402/polar.v33.21004

Meier WN and Stewart JS (2019) Assessing uncertainties in sea ice extent climate indicators. *Environmental Research Letters* 14, 035005.

Nihashi S and Cavalieri D (2006) Observational evidence of a hemispheric-wide ice–ocean albedo feedback effect on Antarctic sea-ice decay. *Journal Geophysical Research* 111(C12001). doi: 10.1029/2005JC003447

Nihashi S and Ohshima K (2001) Relationship between ice decay and solar heating through open water in the Antarctic sea ice zone. *Journal of Geophysical Research: Oceans* 106(C8), 16767–16782. doi: 10.1029/2000JC000399

Parkinson CL (2019) A 40-y record reveals gradual Antarctic sea ice increases followed by decreases at rates far exceeding the rates seen in the Arctic. *Proceedings of the National Academy of Sciences* 116(29), 14414–14423. doi: 10.1073/pnas.1906556116.

Raphael MN (2004) A zonal wave 3 index for the Southern Hemisphere. *Geophysical Research Letters* 31(23), 1–4. doi: 10.1029/2004GL020365

Raphael MN and Hobbs W (2014) The influence of the large-scale atmospheric circulation on Antarctic sea ice during ice advance and retreat seasons. *Geophysical Research Letters* 41(14), 5037–5045.

Raphael MN and Holland MM (2006) Twentieth century simulation of the Southern Hemisphere climate in coupled models. Part 1: large scale circulation variability. *Climate Dynamics* 26(2–3), 217–228. doi: 10.1007/s00382-005-0082-8

Roach LA, Dean SM and Renwick JA (2018) Consistent biases in Antarctic sea ice concentration simulated by climate models. *The Cryosphere* **12**(1), 365–383. doi: 10.5194/tc-12-365-2018

Rosenblum E and Eisenman I (2017) Sea ice trends in climate models only accurate in runs with biased global warming. *Journal of Climate* **30**(16), 6265–6278. doi: 10.1175/JCLI-D-16-0455.1

Swart NC, Fyfe JC, Hawkins E, Kay JE and Jahn A (2015) Influence of internal variability on Arctic sea-ice trends. *Nature Climate Change* **5**(2), 86–89.

Turner J, Bracegirdle TJ, Phillips T, Marshall GJ and Hosking JS (2013) An initial assessment of Antarctic sea ice extent in the CMIP5 models. *Journal of Climate* **26**(5), 1473–1484.

Turner J, Marshall G and Lachlan-Cope T (1998) Analysis of synoptic-scale low pressure systems within the Antarctic Peninsula sector of the circumpolar trough. *International Journal of Climatology* **18**(3), 253–280. doi: 10.1002/(SICI)1097-0088(19980315)18:3<253::AID-JOC248>3.0.CO;2-3

van Loon H (1967) The half-yearly oscillations in Middle and High Southern Latitudes and the coreless winter. *Journal of the Atmospheric Sciences* **24**, 472–486. doi: 10.1175/1520-0469(1967)024<0472:THYOIM>2.0.CO;2

Vichi M and 14 others (2019) Effects of an explosive polar cyclone crossing the antarctic marginal ice zone. *Geophysical Research Letters* **46**(11), 5948–5958. doi: 10.1029/2019GL082457